

Semantic Feature Division Multiple Access for Digital Semantic Broadcast Channels

Shuai Ma, *Member, IEEE*, Zhiye Sun, Bin Shen, Youlong Wu, *Member, IEEE*, Hang Li, *Member, IEEE*, Guangming Shi, *Fellow, IEEE*, Shiyin Li, and Naofal Al-Dhahir, *Fellow, IEEE*

Abstract—In this paper, we propose a digital semantic feature division multiple access (SFDMA) paradigm in multi-user broadcast (BC) networks for the inference and the image reconstruction tasks. In this SFDMA scheme, the multi-user semantic information is encoded into discrete approximately orthogonal representations, and the encoded semantic features of multiple users can be simultaneously transmitted in the same time-frequency resource. Specifically, for inference tasks, we design a SFDMA digital BC network based on robust information bottleneck (RIB), which can achieve a tradeoff between inference performance, data compression and multi-user interference. Moreover, for image reconstruction tasks, we develop a SFDMA digital BC network by utilizing a Swin Transformer, which significantly reduces multi-user interference. More importantly, SFDMA can protect the privacy of users’ semantic information, in which each receiver can only decode its own semantic information. Furthermore, we establish a relationship between performance and signal to interference plus noise ratio (SINR), which is fitted by an Alpha-Beta-Gamma (ABG) function. Furthermore, an optimal power allocation method is developed for the inference and reconstruction tasks. Extensive simulations verify the effectiveness and superiority of our proposed SFDMA scheme.

Index Terms—Semantic broadcast network, semantic feature division multiple access, image reconstruction.

I. INTRODUCTION

With the unprecedented increase of various intelligent applications, such as massive Internet of Things (IoT), multi-sensory extended reality (XR), autonomous driving, flying vehicles, and holographic communication [3], it is envisioned that the fifth-generation (5G) wireless communication is approaching the Shannon limits [4], and reaching a resource bottleneck for the massive connectivity requirements [5], [6]. Efficient multiple access schemes are the key solutions to increase the massive connectivity with high spectral efficiency.

From the first generation (1G) to 5G, orthogonal multiple access (OMA) schemes schedule users or groups of users in orthogonal dimensions [7], including frequency division multiple access (FDMA), time division multiple access (TDMA), code division multiple access (CDMA), orthogonal frequency division multiple access (OFDMA), and space division multiple access (SDMA), which can prevent inter-user interference with low complexity. In addition, the non-orthogonal multiple access (NOMA) [8], which utilizes the superposition coding (SC) at transmitters and the successive interference cancellation (SIC) at receivers, has been proposed to superpose users in the same time-frequency resource. Due to the high SIC

complexity, the number of superposition users in the same time-frequency resource is limited to two [9], which restricts the achievable rates. Thus, 6G needs to explore new degree of freedom to satisfy the massive connectivity [10], [11].

Fortunately, with the successful development of deep learning (DL), the semantic communication, which is inspired from the human-to-human communication, has the potential to address the technological challenges in the existing wireless network. In contrast to the traditional communications, which increase the transmission rate by increasing the physical resource consumption, such as bandwidth, antennas and transmit power, semantic communications focus on transmitting only task-related information, which can significantly reduce the data traffic. By exploiting the computing power to alleviate the cost of the communication resources [12]–[14], semantic communication is a promising paradigm shift for the 6G wireless network design.

In general, there are two typical application tasks of semantic communications, i.e., inference tasks and data reconstruction tasks. Specifically, for inference tasks, semantic communications focus on only transmitting the information with the specific meanings for various tasks [15]–[19], instead of accurate data recovery. For example, a masked vector quantized-variational auto-encoder (VQ-VAE) method was proposed in [17] to improve robustness against semantic noise. For downstream inference tasks, a variational information bottleneck (VIB) [20] based semantic encoding approach was proposed in [18] to reduce the feature transmission latency in dynamic channel conditions. Furthermore, a robust VIB based digital semantic communications was designed in [19] that can achieve better inference performance than the baseline methods with low communication latency.

For data reconstruction tasks, various deep joint source-channel coding (JSCC) semantic communication schemes were designed for different data modalities, such as text [12], [21], [22], speech [13], [23], image [24]–[26] and video [27], [28]. More specifically, for text transmission, a transformer based on semantic coding scheme was proposed in [12] by using sentence similarity to deal with channel noise and semantic distortion. To accurately recover speech information at the semantic level, a DL-enabled semantic communication system was designed in [13] by employing a squeeze-and-excitation (SE) network, which is robust to channel variations for low signal-to-noise (SNR) regions. For wireless image transmission, a reinforcement learning based adaptive semantic coding (RL-ASC) scheme was designed in [16] for image reconstruction with high semantic similarity and perceptual

Shuai Ma is with Peng Cheng Laboratory, Shenzhen 518066, China. (e-mail: mash01@pcl.ac.cn).

performance. For wireless video conferencing, an incremental redundancy hybrid automatic repeatrequest (IR-HARQ) framework was presented in [29] that the channel state information (CSI) is considered to allocate the key point transmission and enhance the performance dramatically. However, the above existing semantic communication works only focus on the single-user scenarios, which cannot be directly applied in the multi-user broadcast communication (BC) network, due to the single-user semantic coding schemes cannot effectively deal with the multi-user interference.

Note that the multi-user semantic BC networks, as the most common communication scenario, are still not well studied. Different from the single-user semantic communication scenarios, the multi-user interference is a critical bottleneck for improving the capacity of multi-user communication networks.

Based on the deep neural network (DNN), the authors of [30] designed a semantic communication system for the broadcast scenario, where the two receivers use semantic recognizer to distinguish positive and negative sentences. For visual question answering (VQA) tasks, a multi-user task-oriented communication system was developed in [31] by using multiple antennas linear minimum mean-squared error (L-MMSE) detector and joint source channel decoder, to mitigate the effects of channel distortion and inter-user interference. Moreover, in [32], a multi-user semantic communication system is studied to execute object-identification tasks, where correlated source data among different users is transmitted via a shared channel. By combining the similar components of the extracted semantic features, a model division multiple access (MDMA) scheme was proposed in [33], in which the common semantic information of multi-user is transmitted within the same time-frequency resources and the personalized semantic information is transmitted separately. In [34], the authors proposed a multi-modal information fusion scheme for multi-user semantic communications, where the wireless channel acts as a medium to fuse multi-modal data where a receiver retrieves semantic information without the need to perform multiuser signal detection. By using attention and residual structure modules, a DL-based multiple access method was designed in [35] for continuous semantic symbols analog transmission in image reconstruction tasks.

In the above existing works [30]–[35], JSCC directly maps the source data into continuous channel input symbols, which is incompatible with current digital communication systems. Moreover, the direct transmission of continuous feature representations requires analog modulation or a full-resolution constellation, which brings huge burdens for resource-constrained radio frequency systems. In addition, the performance of semantic communication depends on transmission power. The existing semantic communication performance measurements are end-to-end, such as classification accuracy for inference tasks, which has no consideration of transmission power. The main reason is that DL based semantic encoders are generally highly complex nonlinear functions, and it is hard to derive analytical relationships between end-to-end performance measures related to the transmit power. Therefore, there is no theoretical basis for adaptive power control for semantic communications, which leads to performance degradation in

random fading channels.

In short, mitigating the multi-user interference and missing theoretical model for adaptive power allocation in the semantic communication are the two major research challenges. In this paper, we explore a new resource domain—semantic feature domain, and propose a semantic feature division multiple access (SFDMA) scheme, where the information of multiple users are encoded in the distinguishable feature subspaces. Specifically, in proposed SFDMA scheme, the encoded semantic features of multiple users are approximately orthogonal to each other, and can be simultaneously transmitted in the same time-frequency resource. This scheme is applied in two scenarios: one focused on inference tasks and the other on image reconstruction. The main contributions of this paper can be summarized as follows:

- By exploring the feature domain, we propose a SFDMA scheme for multi-user BC networks, in which the base station (BS) encodes the multi-user information into discrete semantic feature representations, ensuring semantic features of different users are approximately orthogonal, which effectively alleviates multi-user interference.
- For inference tasks, we design a SFDMA BC network based on a robust information bottleneck (RIB), which can achieve a tradeoff between inference performance, data compression and multi-user interference. Specifically, by exploiting RIB, the SFDMA BC network maximizes the semantic coded redundancy for robust transmission, while restricting the multi-user interference and extract sufficient semantic information for the inference tasks. Due to the computational intractability of mutual information, we derive the tractable variational upper bound of the RIB by utilizing the variational approximation technique. The proposed RIB based SFDMA scheme can achieve efficient transmission of the semantic information, while protecting user semantic information from being decoded by other users.
- For image reconstruction tasks, we design a SFDMA BC network based on the Swin Transformer, a novel and effective computer vision model [36]. The network broadcasts discrete multi-user information at the same time and frequency resource. Moreover, our proposed SFDMA scheme protects the privacy of users' semantic information being decoded by other users.
- Furthermore, we establish a relationship between performance and signal to interference plus noise ratio (SINR), which we approximately fit to an Alpha-Beta-Gamma (ABG) formula. To the best of our knowledge, this is the first analytical expression between performance and SINR for semantic BC networks. Based on the ABG function, we propose an optimal power allocation method for the semantic BC network with inference and reconstruction tasks. Our proposed power allocation method can effectively guarantee the quality of service (QoS) semantic communication in random fading channels.

The rest of this paper is organized as follows. Section II and III present the SFDMA BC network with inference and image reconstruction tasks, respectively. Section IV presents

the optimal power allocation scheme for the SFDMA BC network. Then, the extensive simulation results are presented in Section V, followed by the concluding remarks in Section VI.

Notations: Vectors and matrices are represented by bold-faced lowercase and uppercase letters, respectively. The symbols $\mathbb{E}\{\cdot\}$, $(\cdot)^T$, represent the expectation, transpose, respectively. $I(X;Y)$ denotes the mutual information between input X and output Y , and \mathbf{I} is an identity matrix.

TABLE I: Summary of Key Notations

Notations	Meanings
\mathbf{s}_i	The input data of User i
\mathbf{u}_i	The semantic information of User i
\mathbf{a}_i	The extracted semantic features vectors of User i
\mathbf{z}_i	Quantized signal of User i
\mathbf{x}_i	Modulation signal of User i
$f_{\varphi_i}(\cdot)$	The semantic encoder and its parameters φ_i at the BS of User i
$\Psi_i(\cdot)$	Quantizer of User i
$\Theta_m^i(\cdot)$	Modulation of User i
$f_{\psi_i}(\cdot)$	The encoder and its parameters ψ_i of User i
$f_{\theta_i}(\cdot)$	The decoder and its parameters θ_i of User i
\mathbf{y}_i	The signal received by User i
$\hat{\mathbf{u}}_i$	Estimated semantic information of User i
d	Dimension of feature vector

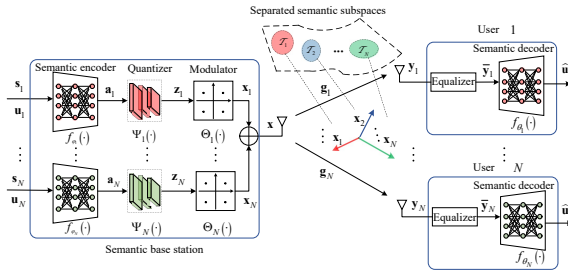


Fig. 1: A digital SFDMA BC network model

II. SFDMA FOR TASK-ORIENTED SEMANTIC BC NETWORK

In this section, we present the SFDMA for task-oriented semantic BC network, and in the section, we devote three subsections to an overview of the task-oriented network model, SFDMA and RIB.

A. Multi-user semantic BC network

Considering a task-oriented multi-user semantic BC network, as depicted in Fig. 1, where a BS aims to transmit the data $\{\mathbf{s}_i\}_{i=1}^N$ with implicit semantic information $\{\mathbf{u}_i\}_{i=1}^N$ to N users simultaneously for inference tasks, and \mathbf{u}_i denotes the intended semantic information of User i , where $i = 1, \dots, N$. Note that in the structure, the encoder f_{ψ_i} is the neural network used for the entire encoding process. In the encoder, the semantic encoder f_{φ_i} is the first module in the encoder used to extract analog semantic features.

To extract the semantic information \mathbf{u}_i , we design a semantic encoder network $f_{\varphi_i}(\cdot)$, which extracts semantic feature \mathbf{a}_i from the source data \mathbf{s}_i as follows

$$\mathbf{a}_i = f_{\varphi_i}(\mathbf{s}_i), \quad i \in \{1, \dots, N\}. \quad (1)$$

Note that, the feature representations $\{\mathbf{a}_i\}_{i=1}^N$ are continuous, and the direct transmission of continuous feature representation needs to be modulated with analog modulation or a full-resolution constellation, which brings huge burdens for resource-constrained transmitter and poses implementation challenges on the current radio frequency (RF) systems. Thus, the continuous feature representations \mathbf{a}_i are quantized as follows

$$\mathbf{z}_i = \Psi_i(\mathbf{a}_i), \quad i \in \{1, \dots, N\}, \quad (2)$$

where $\Psi_i(\cdot)$ denotes the quantizer for \mathbf{a}_i . Specifically, this quantizer transforms the real-valued input into a discrete set of values, typically +1 and -1, according to the sign of the input. This deterministic binarization allows the network to perform efficient binary operations while preserving the ability to propagate gradients using straight-through estimator (STE) [37]. Then, the quantized signal \mathbf{z}_i is modulated and power normalized, i.e.,

$$\mathbf{x}_i = \Theta_i(\mathbf{z}_i), \quad i \in \{1, \dots, N\}, \quad (3)$$

where $\Theta_i(\cdot)$ denotes the modulator and power normalizer for \mathbf{z}_i . In this work, binary phase shift keying (BPSK) modulation is employed.

Then, by applying power amplification, the transmitter broadcasts the semantic encoding information $\{\mathbf{x}_i\}_{i=1}^N$ to the N users. The received signal of User i is given as

$$\mathbf{y}_i = \underbrace{\mathbf{g}_i \sqrt{p_i} \odot \mathbf{x}_i}_{\text{desired signal}} + \underbrace{\mathbf{g}_i \sum_{j=1, j \neq i}^N \sqrt{p_j} \odot \mathbf{x}_j}_{\text{interference}} + \underbrace{\mathbf{n}_i}_{\text{noise}}, \quad i \in \{1, \dots, N\}, \quad (4)$$

where \mathbf{g}_i is channel gain between BS and User i , p_i is the allocated transmitted power for the signal \mathbf{x}_i , and $\mathbf{n}_i \sim \mathcal{CN}(0, \sigma_i^2 \mathbf{I})$ denotes the received additive white Gaussian noise of User i , $\mathbf{g}_i \mathbf{x}_i$ is the desired signal of User i , $\mathbf{g}_i \sum_{j=1, j \neq i}^N \mathbf{x}_j$ is the multi-user semantic interference.

By applying the equalizer, the equalized received signal $\bar{\mathbf{y}}_i$

is given as

$$\bar{\mathbf{y}}_i = \sqrt{p_i} \mathbf{x}_i + \sum_{j=1, j \neq i}^N \sqrt{p_j} \mathbf{x}_j + \frac{\mathbf{n}_i}{\mathbf{g}_i}, i \in \{1, \dots, N\}, \quad (5)$$

where $\bar{\mathbf{y}}_i$ is decoded by $f_{\theta_i}(\cdot)$

$$\hat{\mathbf{u}}_i = f_{\theta_i}(\bar{\mathbf{y}}_i), i \in \{1, \dots, N\}, \quad (6)$$

where \mathbf{u}_i is the inference information of u_i .

B. SFDMA for BC networks

Note that, in contrast to the single user point-to-point semantic communication without user interference, in multi-user semantic BC networks, the BS sends the semantic information of multiple users to each user at the same time-frequency resources, and multi-user interference is a key bottleneck that restricts the transmission rate and QoS.

To overcome this bottleneck, we propose a SFDMA scheme for semantic BC networks. Specifically, via the encoder $f_{\psi}(\cdot)$, the multi-user data $\{\mathbf{s}_i\}_{i=1}^N$ are encoded to discrete semantic features $\{\mathbf{x}_i\}_{i=1}^N$, i.e.,

$$\{\mathbf{x}_1, \dots, \mathbf{x}_N\} = f_{\psi}(\mathbf{s}_1, \dots, \mathbf{s}_N, \mathbf{g}_1, \dots, \mathbf{g}_N), \quad (7)$$

where \mathbf{g}_i denotes the channel gain from the BS to the user i , $i \in \{1, \dots, N\}$.

In the SFDMA scheme, the semantic features of multi-user are approximately orthogonal, i.e.,

$$\frac{\mathbf{x}_i^H \mathbf{x}_j}{\|\mathbf{x}_i\| \|\mathbf{x}_j\|} \rightarrow 0, \forall i \neq j. \quad (8)$$

Since the semantic encoded vectors of users are mutually orthogonal, the semantic information of multiple users can be transmitted simultaneously on same time-frequency resources, avoiding interference among users. In addition, SFDMA can achieve a certain degree of semantic information privacy protection, that is, users can only decode their own semantic information and cannot decode the semantic information of other users.

C. RIB principle

For inference tasks, the more semantic data is transmitted to the users, the more accurate inference can be attained. However, more data transmission will increase communication overhead and interference to other users. As a result, there is an inherent trade-off among inference performance, data compression and multi-user interference. Such a trade-off is a key factor in inference task-oriented communication design. To achieve the above trade-off, we formulate SFDMA BC for inference tasks problem based on RIB principle, which concludes three mutual information terms. Note that the mutual information quantifies the amount of information shared between two random variables, indicating the extent of their dependency. Its physical significance lies in measuring the

reduction in uncertainty of one variable upon knowing the other, specifically:

$$\min_{\{p_{\psi_i}(\mathbf{x}_i|\mathbf{s}_i)\}_{i=1}^N} \sum_{i=1}^N -I(U_i; Y_i) - \omega_i [I(X; Y_i) - I(S_i; Y_i)], \quad (9)$$

where $\omega_i > 0$ is a weighted parameter, $I(U_i; Y_i)$ denotes the mutual information between the received signal Y_i and the semantic information U_i , higher mutual information indicates better inference performance, $I(X; Y_i)$ denotes the mutual information between the received signal Y_i and the transmitted signal X , $I(S_i; Y_i)$ denotes the mutual information between the received signal Y_i and the source signal S_i . The term $I(X; Y_i) - I(S_i; Y_i)$ represents the redundant information in the transmitted signal compared to the source signal, which helps to overcome noise and multi-user interference.

Let \mathcal{L}_{RIB} denote the objective function of the optimization problem (9), which can be equivalently reformulated as

$$\begin{aligned} \mathcal{L}_{\text{RIB}} &= \sum_{i=1}^N \mathbb{E}_{p(\mathbf{s}_i, \mathbf{u}_i)} \left\{ \mathbb{E}_{p_{\psi_i}(\mathbf{y}_i|\mathbf{s}_i)} [-\log p_{\psi_i}(\mathbf{u}_i|\mathbf{y}_i)] \right. \\ &\quad \left. + \omega_i \mathbb{E}_{p_{\psi_i}(\mathbf{x}|\mathbf{s}_i)} [H(Y_i|\mathbf{x})] - \omega_i H_{\psi_i}(Y_i|\mathbf{s}_i) - H(U_i) \right\} \\ &= \sum_{i=1}^N \mathbb{E}_{p(\mathbf{s}_i, \mathbf{u}_i)} \left\{ \mathbb{E}_{p_{\psi_i}(\mathbf{y}_i|\mathbf{s}_i)} [-\log p_{\psi_i}(\mathbf{u}_i|\mathbf{y}_i)] \right. \\ &\quad \left. + \omega_i \mathbb{E}_{p_{\psi_i}(\mathbf{x}|\mathbf{s}_i)} [H(Y_i|\mathbf{x})] - \omega_i H_{\psi_i}(Y_i|\mathbf{s}_i) \right\}, \quad (10) \end{aligned}$$

where $H(U_i)$ is ignored in (10) since it is constant.

However, the calculation of the posterior $p_{\psi_i}(\mathbf{u}_i|\mathbf{y}_i)$ in (10) involves high-dimensional integrals, i.e.,

$$\begin{aligned} p_{\psi_i}(\mathbf{u}_i|\mathbf{y}_i) &= \frac{\int p_{\psi_i}(\mathbf{s}_i, \mathbf{u}_i) p_{\psi_i}(\mathbf{y}_i|\mathbf{s}_i) d\mathbf{s}_i}{p_{\psi_i}(\mathbf{y}_i)} \\ &= \frac{\int p_{\psi_i}(\mathbf{s}_i, \mathbf{u}_i) p_{\psi_i}(\mathbf{y}_i|\mathbf{s}_i) d\mathbf{s}_i}{\int p_{\psi_i}(\mathbf{s}_i, \mathbf{u}_i) p_{\psi_i}(\mathbf{y}_i|\mathbf{u}_i) d\mathbf{u}_i d\mathbf{s}_i}. \quad (11) \end{aligned}$$

To address this challenge, we exploit variational distributions $q_{\theta_i}(\mathbf{y}_i)$ and $q_{\theta_i}(\mathbf{u}_i|\mathbf{y}_i)$ to approximate the distributions $p(\mathbf{y}_i)$ and $p(\mathbf{u}_i|\mathbf{y}_i)$, respectively [38], where θ_i is the parameter of semantic decoder of User i , and is used to compute the inference result $\hat{\mathbf{u}}_i$. Specifically, the upper bound of the first term $\mathbb{E}_{p(\mathbf{s}_i, \mathbf{u}_i)} \left\{ \mathbb{E}_{P_{\psi_i}(\mathbf{y}_i|\mathbf{s}_i)} [-\log p_{\psi_i}(\mathbf{u}_i|\mathbf{y}_i)] \right\}$ of (10) is given as

$$\begin{aligned} &\mathbb{E}_{p(\mathbf{s}_i, \mathbf{u}_i)} \left\{ \mathbb{E}_{p_{\psi_i}(\mathbf{y}_i|\mathbf{s}_i)} [-\log p_{\psi_i}(\mathbf{u}_i|\mathbf{y}_i)] \right\} \\ &= \mathbb{E}_{p(\mathbf{s}_i, \mathbf{u}_i)} \left\{ \mathbb{E}_{p_{\psi_i}(\mathbf{y}_i|\mathbf{s}_i)} [-\log q_{\theta_i}(\mathbf{u}_i|\mathbf{y}_i)] \right. \\ &\quad \left. - D_{\text{KL}}(p_{\psi_i}(\mathbf{s}_i|\mathbf{y}_i) \| q_{\theta_i}(\mathbf{s}_i|\mathbf{y}_i)) \right\} \quad (12a) \end{aligned}$$

$$\leq \mathbb{E}_{p(\mathbf{s}_i, \mathbf{u}_i)} \left\{ \mathbb{E}_{p_{\psi_i}(\mathbf{y}_i|\mathbf{s}_i)} [-\log q_{\theta_i}(\mathbf{u}_i|\mathbf{y}_i)] \right\}, \quad (12b)$$

where D_{KL} represents the Kullback-Leibler divergence, which is a measure of the difference between two probability distributions, thus the inequality (12b) holds due to $D_{\text{KL}} \geq 0$.

Moreover, since \mathbf{y}_i is corrupted by channel noise and multi-user interference, we can derive a lower bound for the entropy

term $H_{\psi_i}(Y_i|\mathbf{s}_i)$ as

$$H_{\psi_i}(Y_i|\mathbf{s}_i) \geq H_{\psi_i}(X_i|\mathbf{s}_i). \quad (13)$$

Hence, the objective function in (10) is upper bounded by

$$\begin{aligned} \mathcal{L}_{\text{RIB}} \leq & \sum_{i=1}^N \mathbb{E}_{p(\mathbf{s}_i, \mathbf{u}_i)} \left\{ \mathbb{E}_{P_{\psi_i}(\mathbf{y}_i|\mathbf{s}_i)} [-\log q_{\theta_i}(\mathbf{u}_i|\mathbf{y}_i)] \right. \\ & \left. + \omega_i \mathbb{E}_{P_{\psi_i}(\mathbf{x}|\mathbf{s}_i)} [H(Y_i|\mathbf{x})] - \omega_i H_{\psi_i}(Y_i|\mathbf{s}_i) \right\} \quad (14) \end{aligned}$$

The conditional entropy terms $H_{\psi_i}(Y_i|\mathbf{s}_i)$ and $H(Y_i|\mathbf{x})$ in (14) are analytically computable with respect to the parameters ψ_i . The DNN-based encoder is defined by the factorial distribution $p_{\psi_i}(\mathbf{y}_i|\mathbf{s}_i) = \prod_{j=1}^d p_{\psi_i}(y_{i,j}|\mathbf{s}_i)$. Specifically, the entropy terms can be decomposed into the following summations:

$$H_{\psi_i}(Y_i|\mathbf{s}_i) = \sum_{j=1}^d H_{\psi_i}(Y_{i,j}|\mathbf{s}_i), \quad (15a)$$

$$H(Y_i|\mathbf{x}) = \sum_{j=1}^d H_j(Y_{i,j}|\mathbf{x}_j). \quad (15b)$$

By further applying Monte Carlo sampling, we are able to obtain an unbiased estimate of the gradient and hence optimize the objective using stochastic gradient descent. We have the following empirical estimation:

$$\begin{aligned} \mathcal{L}_{\text{RIB}} \leq & \sum_{i=1}^N \frac{1}{M} \sum_{m=1}^M \left\{ \frac{1}{L} \sum_{l=1}^L [-\log q_{\theta_i}(\mathbf{u}_i^{(m)}|\mathbf{y}_i^{(m,l)})] \right. \\ & \left. + \omega_i \sum_{j=1}^d H(Y_{i,j}|\mathbf{x}_j^{(m,l)}) - \omega_i \sum_{j=1}^d H_{\psi_i}(Y_{i,j}|\mathbf{s}_i^{(m)}) \right\}, \quad (16) \end{aligned}$$

where M is the batch size of training dataset, L is the sample times for each pair $\{(\mathbf{s}_i^{(m)}, \mathbf{u}_i^{(m)})\}_{m=1}^M$, and d represents the dimension of signal vector Y and X .

The first term $-\log q_{\theta_i}(\mathbf{u}_i^{(m)}|\mathbf{y}_i^{(m,l)})$, is maximized, which is equivalent to minimizing the cross-entropy between \mathbf{u}_i and $\hat{\mathbf{u}}_i$. The second term $H(Y_{i,j}|\mathbf{x}_j^{(m,l)})$ can be computed for different discrete value of \mathbf{x}_j , the conditional distribution $p(\mathbf{y}_i|\mathbf{x})$ depends on the allocated transmitted power p_i , where $i = 1, 2, \dots, N$, and the noise variance σ^2 , as shown in (5). The third term $H_{\psi_i}(Y_{i,j}|\mathbf{s}_i^{(m)})$ is determined by $p(\mathbf{y}_{i,j}|\mathbf{s}_i)$. Specifically, we model the conditional distribution $p_{\varphi}(\mathbf{a}_{i,j}|\mathbf{s}_i)$ as a multivariate Gaussian distribution due to the feature of neural network, combined with the binarized quantification method and the BPSK modulation, the conditional distribution $p_{\psi}(\mathbf{x}_{i,j}|\mathbf{s}_i)$ is modeled as a uniform Bernoulli distribution, then $p(\mathbf{y}_{i,j}|\mathbf{s}_i)$ is depicted as:

$$\begin{aligned} p_{\psi}(\mathbf{y}_{i,j}|\mathbf{s}) = & \sum_{t=1}^T \frac{1}{T} f_{\varepsilon}(\sqrt{p_i} \mathbf{x}_{i,j} + \sum_{c=1, c \neq i}^N \sqrt{p_c} \mathbf{x}_{c,j} \\ & + \frac{\mathbf{n}_{i,j}}{\mathbf{g}_{i,j}} - q_t), \quad (17) \end{aligned}$$

where T denotes quantization bits and q_t represents the quantized discrete value. Since we have used binarized quantization

method, T is set to 2 and $q_t \in \{-1, 1\}$. f_{ε} denotes the density function of ε , where $\varepsilon = \sqrt{p_i} \mathbf{x}_{i,j} + \sum_{c=1, c \neq i}^N \sqrt{p_c} \mathbf{x}_{c,j} + \frac{\mathbf{n}_{i,j}}{\mathbf{g}_{i,j}} - q_t$, which follows a distribution that combined with the known Bernoulli distribution and Cauchy distribution.

The training procedures of the SFDMA scheme is summarized in Algorithm 1.

Algorithm 1: The proposed training algorithm for SFDMA BC network with inference tasks

Input: T (number of epochs), L (number of encoding representation samples per data sample)

```

1 for epoch  $t = 1$  to  $T$  do
2   Sample mini-batch of data samples  $\{(\mathbf{s}_i, \mathbf{u}_i)\}_{i=1}^N$ 
   from each BS;
3   Compute conditional distribution  $p_{\phi_i}(\mathbf{y}_i|\mathbf{s}_i)$ ;
4   Compute the conditional entropy term
    $H_{\phi_i}(Y_{i,j}|\mathbf{s}_i)$ ;
5   Quantize the discrete representation  $\{z_j^{(i,l)}\}_{l=1}^L$ 
   based on Eq. (2);
6   Compute the entropy terms  $\{H(Y_{i,j}|\mathbf{x}_j^{(i,l)})\}_{l=1}^L$ ;
7   Sample the noise  $\{\epsilon^{(i,l)}\}_{l=1}^L \sim \mathcal{CN}(0, \sigma^2 \mathbf{I})$ ;
8   Estimate the corrupted discrete representation
    $\{\mathbf{y}_j^{(i,l)}\}_{l=1}^L$ ;
9   Compute the loss  $\mathcal{L}_{VRIB}(\phi_i, \theta_i)$  based on
   Eq. (16);
10  Update the parameters  $\phi_i$  and  $\theta_i$  through
   backpropagation;
11 end

```

The training process not only minimizes semantic decoding error but also implicitly fosters the orthogonality of the encoded signals. On one hand, during joint training, the SFDMA naturally learns to semantic encoding such that the outputs are as different as possible to reduce redundancy. This drives the semantic encoded signals towards orthogonality, as orthogonal signals do not interfere with each other, allowing the decoders to separate them more easily. As training progresses, gradient descent optimization will push the semantic encoded signals towards directions that minimize mutual interference, eventually leading them towards an orthogonal solution. This is a spontaneous mechanism where, even without explicit orthogonality constraints, the training process reduces correlation between signals to minimize reconstruction error.

On the other hand, orthogonality reduces interference. Specifically, orthogonal signals have a zero inner product, meaning they do not overlap in signal space. By encouraging orthogonality, the system can minimize interference, improving decoder performance and making it easier to recover the original inputs. The loss function aims to minimize the semantic decoding error. Given the received signals, if the semantic encoded signals interfere too much, it will result in poor reconstruction, increasing the loss. To minimize the loss, the training process will encourage the encoders to produce

the semantic encoded signals that are well-separated in signal space, thus driving them toward orthogonality.

III. SFDMA FOR IMAGE RECONSTRUCTION SEMANTIC BC NETWORK

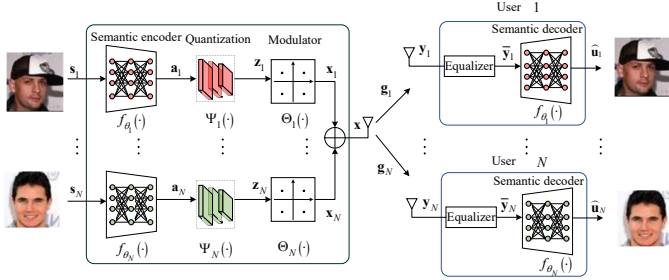


Fig. 2: A SFDMA BC network for image reconstruction

Furthermore, we investigate SFDMA scheme for multi-user semantic BC networks with image reconstruction tasks. Specifically, as shown in Fig. 2, by exploiting the SFDMA scheme, a semantic BS aims to transmit images $\{s_i\}_{i=1}^N$ to N users simultaneously, where s_i is the intended image of User i , $i = 1, \dots, N$. The semantic BS includes semantic encoders $f_{\phi_i}(\cdot)$, quantizers $\Psi_i(\cdot)$ and modulators $\Theta_i(\cdot)$.

Fig. 3(a) shows the architecture of the semantic encoder of $f_{\phi_i}(\cdot)$ for User i with the parameter set ϕ_i . The semantic encoder $f_{\phi_i}(\cdot)$ includes three layers, where the dimensions are 128, 256 and 512, respectively.

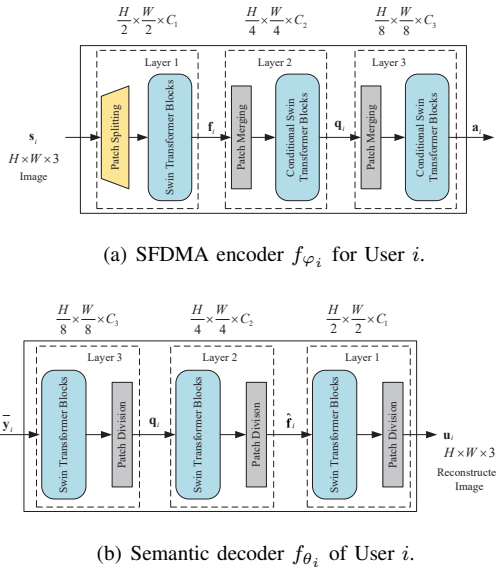


Fig. 3: (a) The architecture of the semantic encoder f_{ϕ_i} of SFDMA BC network for image reconstruction; (b) The architecture of the semantic decoder of User i for image reconstruction

In Layer 1, an RGB image $s_i \in \mathbb{R}^{3 \times H \times W}$ is first split into $l_1 = \frac{H}{2} \times \frac{W}{2}$ non-overlapping patches. After patch embedding, Swin Transformer blocks are applied to these l_1 non-overlapping patches. Here, we refer to these N_1 blocks together with the patch embedding layer as

$$\mathbf{f}_i = \text{Layer1}(\mathbf{s}_i), \quad (18)$$

where $\mathbf{f}_i \in \mathbb{R}^{\frac{H}{2} \times \frac{W}{2} \times C_1}$ is fed to Layer 2 for down-sampling through a patch merging layer, and the down-sampling data is processed by Swin Transformer blocks, i.e.,

$$\mathbf{q}_i = \text{Layer2}(\mathbf{f}_i), \quad (19)$$

where $\mathbf{q}_i \in \mathbb{R}^{\frac{H}{4} \times \frac{W}{4} \times C_2}$ denotes the output of Layer 2. Furthermore, $\{\mathbf{q}_i\}_{i=1}^N$ are processed by Layer 3, which includes a down-sampling Patch Merging layer and Swin Transformer blocks. Finally, the semantic encoded feature vector $\mathbf{a}_i \in \mathbb{R}^{\frac{H}{8} \times \frac{W}{8} \times C_3}$ is given by

$$\mathbf{a}_i = \text{Layer3}(\mathbf{q}_i). \quad (20)$$

In summary, the semantic encoder of SFDMA scheme can be formulated as

$$\mathbf{a}_i = f_{\phi_i}(s_i), \quad (21)$$

where \mathbf{a}_i is the encoded semantic features vectors from s_i , and $f_{\phi_i}(\cdot)$ is the semantic encoder with the parameter set ϕ_i .

Then, the analog semantic features $\{\mathbf{a}_i\}_{i=1}^N$ are quantized as

$$\mathbf{z}_i = \Psi_i(\mathbf{a}_i), \quad i \in \{1, \dots, N\}, \quad (22)$$

where \mathbf{z}_i is the quantized signal. Then, we adopt BPSK modulation

$$\mathbf{t}_i = \Theta_i(\mathbf{z}_i), \quad i \in \{1, \dots, N\}. \quad (23)$$

Before transmission, we perform normalization processing,

$$\mathbf{x}_i = \frac{\mathbf{t}_i}{\|\mathbf{t}_i\|_2}. \quad (24)$$

For User i , the received signal is computed based on Eq. (4), and then we use Eq. (5) to obtain the equalized signal \bar{y}_i .

Furthermore, the equalized signal \bar{y}_i is sent to semantic decoder $f_{\theta_i}(\cdot)$, as shown in Fig. 3(b), which consists of three layers. Specifically, in Layer 1, the feature vector $\mathbf{y}_i \in \mathbb{R}^{\frac{H}{8} \times \frac{W}{8} \times C_3}$ is first sampled by Swin Transformer blocks. Then by applying a Patch Division layer, we obtain $\hat{\mathbf{q}}_i$ as

$$\hat{\mathbf{q}}_i = \text{Layer3}(\bar{\mathbf{y}}_i). \quad (25)$$

Then, $\hat{\mathbf{q}}_i \in \mathbb{R}^{\frac{H}{4} \times \frac{W}{4} \times C_2}$ is fed to Layer 2, which includes Swin Transformer blocks and an up-sampling Patch Division layer. The output of Layer 2 is given by

$$\hat{\mathbf{f}}_i = \text{Layer2}(\hat{\mathbf{q}}_i), \quad (26)$$

where $\hat{\mathbf{f}}_i \in \mathbb{R}^{\frac{H}{2} \times \frac{W}{2} \times C_1}$ is sent into Swin Transformer blocks and an up-sampling Patch Division layer. The reconstructed image $\hat{u}_i \in \mathbb{R}^{H \times W \times 3}$ is given as

$$\hat{\mathbf{s}}_i = \text{Layer1}(\hat{\mathbf{f}}_i). \quad (27)$$

Therefore, the semantic decoder of User i is given as

$$\hat{\mathbf{s}}_i = f_{\theta_i}(\hat{\mathbf{z}}_i), \quad i \in \{1, \dots, N\}, \quad (28)$$

where $f_{\theta_i}(\cdot)$ denotes the semantic decoder of User i with its parameters θ_i .

Moreover, we adopt the MSE loss function for image

reconstruction of the proposed SFDMA scheme as follows

$$\mathcal{L}(\mathbf{s}_i, \hat{\mathbf{s}}_i) = \frac{1}{n} \sum_{j=1}^n (\mathbf{s}_{i,j} - \hat{\mathbf{s}}_{i,j})^2, \quad (29)$$

where n denotes the number of images. In summary, the training procedure for SFDMA BC network with image reconstruction tasks is summarized in Algorithm 2.

Algorithm 2: Training algorithm for SFDMA BC network with image reconstruction tasks

Input: T (number of epochs), N (number of users), noise \mathbf{n}_i with a fixed SNR value

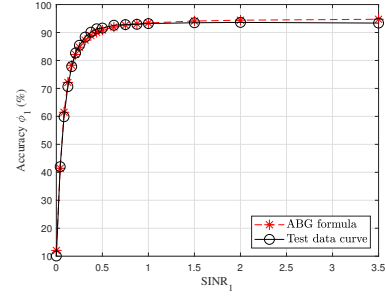
- 1 **for** epoch $t = 1$ **to** T **do**
- 2 **Base station;**
- 3 Sample mini-batch of data samples
 $\{(\mathbf{s}_i, \mathbf{u}_i)\}_{i=1}^N$ from each BS;
- 4 Compute the feature vectors
 $\{f_{\phi_i}(\mathbf{s}_i)\}_{i=1}^N \rightarrow \{\mathbf{a}_i\}_{i=1}^N$;
- 5 Compute the quantized vectors
 $\{\Psi_i(\mathbf{a}_i)\}_{i=1}^N \rightarrow \{\mathbf{z}_i\}_{i=1}^N$;
- 6 Compute the modulation signal
 $\{\Theta_i(\mathbf{z}_i)\}_{i=1}^N \rightarrow \{\mathbf{x}_i\}_{i=1}^N$;
- 7 **Semantic User** i ;
- 8 Compute the equalization received signal
 $\{\mathbf{y}_i\}_{i=1}^N \rightarrow \{\bar{\mathbf{y}}_i\}_{i=1}^N$;
- 9 Image reconstruction $\{f_{\theta_i}(\bar{\mathbf{y}}_i)\}_{i=1}^N \rightarrow \{\hat{\mathbf{s}}_i\}_{i=1}^N$;
- 10 Compute the loss MSE based on Eq. (29);
- 11 Update the parameters ϕ_i and θ_i through backpropagation;
- 12 **end**

IV. OPTIMAL POWER ALLOCATION SCHEME FOR SFDMA BC NETWORK

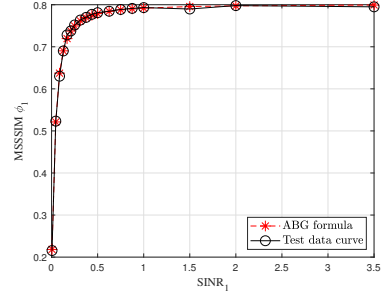
The performance of semantic BC network depends on the transmit power. However, the relationship between the performance of semantic communications and the transmit power has not yet been established, which leads to no theoretical basis for the power allocation for the semantic BC network. To overcome this challenge, we establish the relationship between performance and SINR for the SFDMA BC network.

Let ϕ_i and SINR_i denote the performance and received SINR of User i , respectively. Note that the performance is related to the task at hand, e.g. in image classification tasks the performance metric is accuracy, in image reconstruction tasks the performance is peak signal-to-noise ratio (PSNR) or multiscale structural similarity index metric (MS-SSIM), etc.

With extensive experiments, we find that the performance and SINR satisfies a specific law: *as SINR increases, performance increases rapidly at first, and then slowly increases until it reaches the upper bound*, for example, in the image classification task on the MNIST dataset, the relationship between classification accuracy and SINR is shown in Fig. 4(a). Additionally, the relationship between MS-SSIM and SINR is also illustrated in Fig. 4(b).



(a) ABG formula for inference task.



(b) ABG formula for image reconstruction task.

Fig. 4: Comparison between the ABG formula and the test data curves.

TABLE II: Fitting parameters.

Parameters of ABG formula	α_1	β_1	γ_1	τ_1	ζ
Values	95	15.7	82.93	1.427	0.6338

Therefore, the relationship between ϕ_i and SINR_i of User i can be fitted by ABG function (as shown in Fig. 4) and is given by

$$\phi_i \left(\{p_i\}_{i=1}^N \right) = \alpha_i - \frac{\gamma_i}{1 + (\beta_i \text{SINR}_i)^{\tau_i}}, \quad (30a)$$

$$\text{SINR}_i = \frac{p_i |\mathbf{g}_i|^2}{\sum_{j=1, j \neq i}^N p_j |\mathbf{g}_j|^2 + \sigma_i^2}, \quad (30b)$$

where α_i , β_i , γ_i and τ_i are parameters of the ABG formula. Given the DL based semantic encoders and decoders, the parameters $\{\alpha_i, \beta_i, \gamma_i, \tau_i\}_{i=1}^N$ can be obtained through testing, as listed in Table II.

With the ABG function, we optimize power allocation of the SFDMA BC network to minimize the total power consumption under the performance constraints of the N users. Mathematically, the power allocation optimization problem of the SFDMA BC network can be formulated as

$$\min_{\{p_i\}_{i=1}^N} \sum_{i=1}^N p_i \quad (31a)$$

$$\text{s.t. } \phi_i \left(\{p_i\}_{i=1}^N \right) \geq \eta_i, i = 1, \dots, N, \quad (31b)$$

where η_i denotes the performance requirement of User i .

Furthermore, constraint (31b) can be equivalently reformu-

lated as linear constraint as follows

$$p_i |g_i|^2 \geq \frac{1}{\beta_i} \left(\frac{\gamma_i}{\alpha_i (n_b) - \eta_i} - 1 \right)^{\frac{1}{\tau_i}} \left(\sum_{j=1, j \neq i}^N p_j |g_j|^2 + \sigma_i^2 \right) \quad (32)$$

Thus, the power allocation optimization problem of the SFDMA BC network is a linear programming, which can be efficiently solved by simplex method [39].

Therefore, the workflow of the task-oriented SFDMA BC network is summarized in Algorithm 3.

Algorithm 3: Task-oriented SFDMA BC network workflow

Input: $\{(\mathbf{s}_i, \mathbf{u}_i)\}_{i=1}^N$, N (number of users), $\{\sigma_i^2\}_{i=1}^N$ (noise variance), $\{\mathbf{g}_i^2\}_{i=1}^N$ (channel gain), $\{\psi_i\}_{i=1}^N$ (parameters of encoders), $\{\theta_i\}_{i=1}^N$ (parameters of decoders)

Output: $\{\hat{\mathbf{s}}_i\}_{i=1}^N$ or $\{\hat{\mathbf{u}}_i\}_{i=1}^N$

- 1 Obtain the semantic feature $\{\mathbf{x}_i\}_{i=1}^N$ from the raw data $\{\mathbf{s}_i\}_{i=1}^N$ using the encoder;
 - 2 Compute the allocated power $\{p_i\}_{i=1}^N$ according to Eq. (31a) and (32);
 - 3 Transmit the semantic information of multiple users, the received signal of user i is given as Eq. (5);
 - 4 Equalize the received data according to Eq. (6);
 - 5 **if the current task is an inference task then**
 - 6 Infer the semantic information $\{\hat{\mathbf{u}}_i\}_{i=1}^N$ through the decoder
 - 7 **else**
 - 8 Reconstruct the original data $\{\hat{\mathbf{s}}_i\}_{i=1}^N$ through the decoder
 - 9 **end**
-

V. EXPERIMENTAL RESULTS AND ANALYSIS

A. Experimental Setup

In this section, we perform a comprehensive analysis through the comparison between the proposed SFDMA BC schemes and the conventional deep JSCC schemes [40]. While both use similar neural network designs, the SFDMA BC scheme uniquely incorporates SFDMA, effectively mitigating multi-user interference. The key experimental parameters are shown in Table III.

TABLE III: Key parameters of the SFDMA BC network.

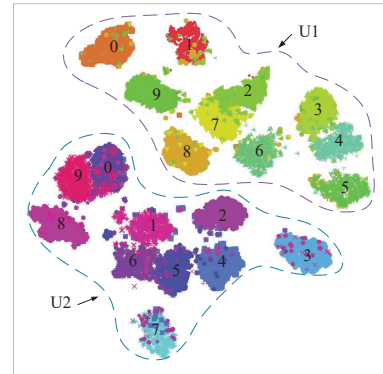
Tasks	Reconstruction	Classification
Batch size	32	512
Latent dimensions	512	1024
Learning rate	1e-4	1e-4
Loss function	MSE	RIB
Training SNR	0dB	0dB
Test metrics	MS-SSIM	Accuracy
Threshold	0.77	92

In inference tasks experiment, the semantic encoder consists of a dense layer and a tanh activation function, and the

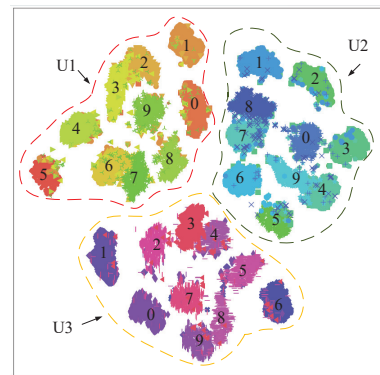
semantic decoders consist of three dense layers, two ReLU as activation function and a softmax function. In the inference tasks networks, the learning rate is $\delta = 10^{-3}$, and the weights of models are updated by the Adam optimizer. The inference tasks experiments are conducted using the widely-used MNIST dataset [41], which comprises a training set of 60,000 sample images and a test set of 10,000 sample images across 10 handwritten digits categories. Meanwhile, the CelebA dataset [42], which includes 202,599 face images and 10,177 celebrity identities, is used for the image reconstruction tasks experiments.

We compare the proposed SFDMA BC scheme with conventional deep JSCC scheme, where the multi-user interference is not ignored during the training phase but is considered during the test phase. Moreover, the deep JSCC scheme without multi-user interference in both training and testing phases are also used for comparison, which is named Upper Bound.

B. Performance evaluation for inference tasks



(a) Two users ($N = 2$).



(b) Three users ($N = 3$).

Fig. 5: Two-dimensional t-SNE embedding of the semantic features $\{\mathbf{x}_i\}_{i=1}^N$ of the proposed SFDMA scheme with $q_{\text{bit}} = 128$ bits and $\text{SNR} = 5\text{dB}$

First, we evaluate the semantic features separation performance of the proposed SFDMA BC scheme by adopting the dimension reduction technique of t-SNE (t-Distributed Stochastic Neighbor Embedding) [43], which is a powerful dimensionality reduction technique that excels in preserving the local structure of high-dimensional data when projecting

it into a lower-dimensional space. By visualizing the semantic encoded feature vectors in 2-dimensional space using t-SNE, we can observe how well-separated the vectors are, which reflects their orthogonality in the original high-dimensional space.

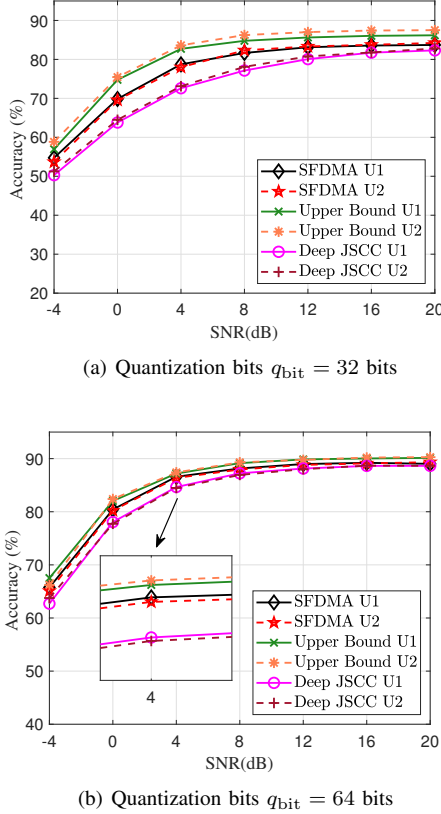


Fig. 6: Performance of classification accuracies over Rayleigh channels with training SNR=0dB.

Fig. 5(a) and 5(b) illustrate two-dimensional t-SNE embedding of the semantic features of the proposed SFMDA BC schemes with two users and three users respectively, where the quantization bits $q_{\text{bit}} = 128$ bits and the training SNR = 5dB. For the two users SFDMA BC network, the classification accuracy of User 1 and 2 are 93.1% and 93.4%, respectively, and for the two users scenario, the classification accuracy of User 1, 2 and 3 are 93.23%, 94.14% and 93.4%, respectively, which demonstrate the effectiveness of the proposed SFDMA scheme. In Fig. 5(a) and 5(b), each point corresponds to the position of a semantic feature in 2-dimensional space obtained through t-SNE, with different colors representing different classes and users. The semantic features belonging to the same user are highlighted by dashed enclosures, the absence of overlap between the semantic features of different users show that the semantic features $\{\mathbf{x}_i\}_{i=1}^N$ are approximately separated, which verifies the approximate orthogonality property of semantic features of the proposed SFDMA scheme.

Table IV illustrates the inner product and the angle among the semantic features \mathbf{x}_1 , \mathbf{x}_2 and \mathbf{x}_3 . Table IV shows that even with the same inputs, the inner products among the semantic features of different users are 1.0×10^{-3} , 2.5×10^{-3} , and

TABLE IV: The inner product and angle among the semantic features $\{\mathbf{x}_i\}_{i=1}^N$ with the same inputs.

Inner product	$\mathbf{x}_1^H \mathbf{x}_2$	$\mathbf{x}_1^H \mathbf{x}_3$	$\mathbf{x}_2^H \mathbf{x}_3$
Value	1.0×10^{-3}	2.5×10^{-3}	2.6×10^{-4}
Angle	$\arccos(\mathbf{x}_1^H \mathbf{x}_2)$	$\arccos(\mathbf{x}_1^H \mathbf{x}_3)$	$\arccos(\mathbf{x}_2^H \mathbf{x}_3)$
Value($^\circ$)	89.94°	89.86°	89.99°

TABLE V: The classification accuracy of the SFDMA BC network with the same inputs.

	$f_{\theta_1}(\mathbf{y}_1)$	$f_{\theta_1}(\mathbf{g}_1, \mathbf{x}_2)$	$f_{\theta_2}(\mathbf{y}_2)$	$f_{\theta_2}(\mathbf{g}_2, \mathbf{x}_1)$
Accuracy(%)	91.91	9.66	91.89	9.71

2.6×10^{-4} , which approach zero. Moreover, the corresponding angles are 89.94° , 89.86° and 89.99° , which approach 90° . The results in Table IV verify the semantic features of multi-user are approximately orthogonal for the proposed SFDMA scheme.

Table V illustrates the classification accuracy of two users with the same inputs. As shown in Table V, even with the same inputs, each user can accurately decode the intended semantic information, and the classification accuracy of User 1 and 2 are 91.91% and 91.89%, respectively. Meanwhile, each user cannot effectively decode the semantic information of other users, i.e., the classification accuracy of User 1 decoding User 2's semantic information is only 9.66%, the classification accuracy of User 1 decoding User 2's semantic information is only 9.71%. The results in Table V also verify the semantic features of multi-user are approximately orthogonal for the proposed SFDMA scheme. Moreover, Table V also demonstrates the proposed SFDMA can provide semantic confidentiality, and protect the semantic information from being decoded by other users.

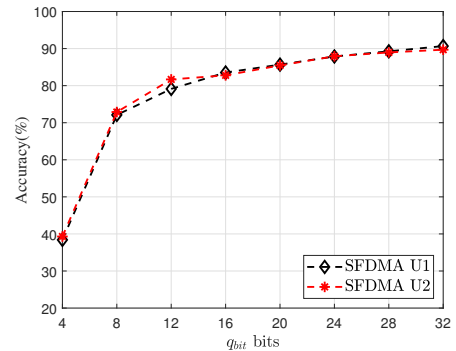
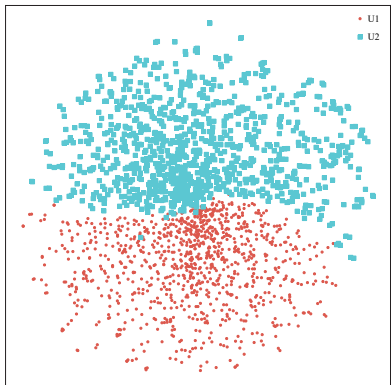


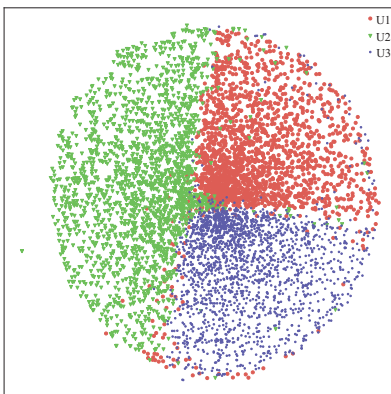
Fig. 7: Performance of classification accuracies versus quantization bit q_{bit} with training SNR=10dB.

Fig. 6(a) and 6(b) illustrate classification accuracies of Deep JSCC, Upper Bound and the proposed SFDMA versus SNR over Rayleigh channel with quantization bits $q_{\text{bit}} = 32$ and 64 bits, respectively, where the training SNR is 0dB. Fig. 6(a) and 6(b) show that, as SNR increases, the classification accuracies of three schemes increase rapidly at first, and then slowly increases until it reaches the maximum value. Moreover, the classification accuracies of the proposed SFDMA scheme are

higher than those of the Deep JSCC and are closer to the Upper Bound in comparison, which verify the proposed SFDMA scheme can effectively eliminate multi-user interference and improve inference tasks performance. Comparing Fig. 6(a) and 6(b), the classification accuracies with quantization bits $q_{\text{bit}} = 64$ bits are higher than that with $q_{\text{bit}} = 32$ bits. Thus, a larger number of quantization bits q_{bit} leads to higher classification accuracy.



(a) PSNR1 = 21, PSNR2 = 21.45, MS-SSIM = 0.802, MS-SSIM = 0.806.



(b) PSNR1 = 24.76dB, PSNR2 = 24.93dB, PSNR3 = 25dB, MS-SSIM1 = 0.907, MS-SSIM2 = 0.909, MS-SSIM3 = 0.91.

Fig. 8: Two-dimensional t-SNE embedding of the received feature in the CelebA reconstruction task.

Fig. 7 shows the classification accuracy versus quantization bits q_{bit} with training SNR = 10dB. It can be seen from Fig. 7 that as quantization bits q_{bit} increases, the classification accuracy increases rapidly at first, and then slowly increases until it reaches the upper bound.

C. Performance Evaluation for Image Reconstruction Tasks

To evaluate the experimental results of image reconstruction, PSNR and MSSIM are employed to measure image reconstruction quality.

Fig. 8(a) and 8(b) illustrate two-dimensional t-SNE embedding of the semantic features of the proposed SFMDA BC

TABLE VI: The inner product and angle among the semantic features of three transmission pairs with the same inputs.

Inner product	$\mathbf{x}_1^H \mathbf{x}_2$	$\mathbf{x}_1^H \mathbf{x}_3$	$\mathbf{x}_2^H \mathbf{x}_3$
Value	-1.0×10^{-3}	7.0×10^{-3}	-2.8×10^{-4}
Angle	$\arccos(\mathbf{x}_1^H \mathbf{x}_2)$	$\arccos(\mathbf{x}_1^H \mathbf{x}_3)$	$\arccos(\mathbf{x}_2^H \mathbf{x}_3)$
Value($^\circ$)	90.06	89.60	90.02

TABLE VII: The image reconstruction of the SFDMA BC network with the same input images.

	$f_{\theta_1}(\mathbf{y}_1)$	$f_{\theta_1}(\mathbf{g}_{1,2}\mathbf{x}_2)$	$f_{\theta_2}(\mathbf{y}_2)$	$f_{\theta_2}(\mathbf{g}_{2,1}\mathbf{x}_1)$
PSNR(dB)	25.72	7.34	25.68	7.20
MS-SSIM	0.928	0.066	0.928	0.057



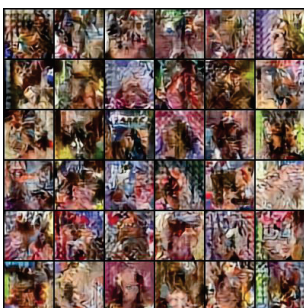
(a) The input images of User 1 and User 2



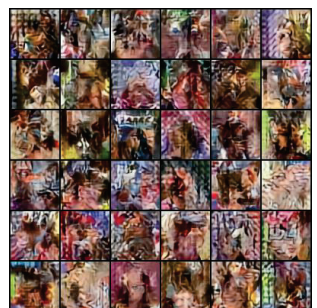
(b) The decoded images of User 1 $f_{\theta_1}(\mathbf{y}_1)$



(c) The decoded images of User 2 $f_{\theta_2}(\mathbf{y}_2)$



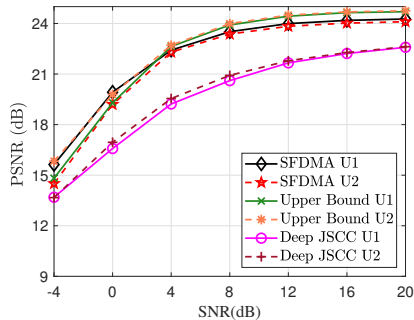
(d) User 1 decoded images of User 2 $f_{\theta_1}(\mathbf{g}_1^H \mathbf{x}_2)$



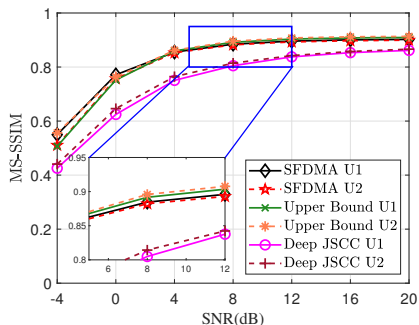
(e) User 2 decoded images of User 1 $f_{\theta_2}(\mathbf{g}_2^H \mathbf{x}_1)$

Fig. 9: The semantic decoded images of User 1 and 2 with the same inputs.

schemes with two users and three users respectively, where the quantization bits $q_{\text{bit}} = 4096$ bits and the training SNR = 5dB. Fig. 8(a) and 8(b) show that the semantic features $\{\mathbf{x}_i\}_{i=1}^N$ are approximately separated, which verifies the approximate



(a) Training SNR = 5dB



(b) Training SNR = 5dB

Fig. 10: PSNR and MS-SSIM of image reconstruction of the semantic BC network over Rayleigh channels.

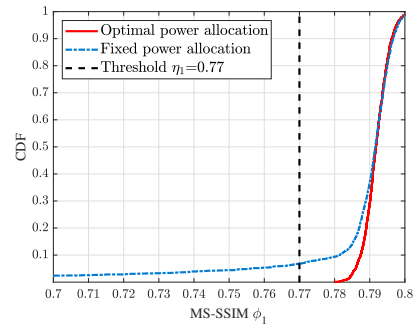
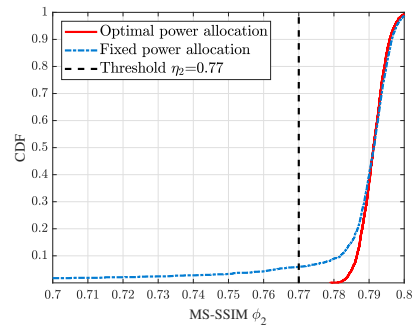
(a) CDF of MS-SSIM ϕ_1 for User 1(b) CDF of MS-SSIM ϕ_2 for User 2

Fig. 13: CDFs of MS-SSIM of User 1 and User 2 with different power allocation methods.

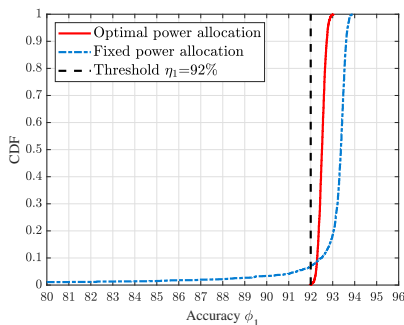
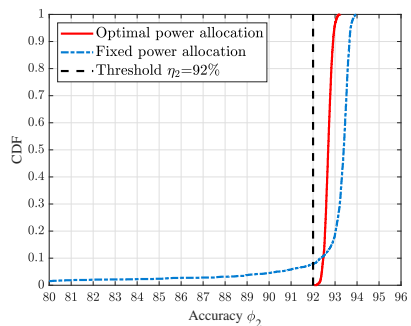
(a) CDF of classification accuracy ϕ_1 for User 1(b) CDF of classification accuracy ϕ_2 for User 2

Fig. 12: CDFs of classification accuracies of User 1 and User 2 with different power allocation methods.

orthogonality property of semantic features of the proposed SFDMA scheme. For the two users scenario, the PSNR of the image reconstruction of User 1 and 2 are 21.00dB and 21.45dB respectively, and the MS-SSIM of the image reconstruction of User 1 and 2 are 0.802 and 0.806, respectively. Moreover, for the three users scenario, the PSNR of the image reconstruction of User 1, 2 and 3 are 24.76dB, 24.93dB and 25.00dB respectively, and the MS-SSIM of the image reconstruction of User 1, 2 and 3 are 0.907, 0.909 and 0.910, respectively.

Table VI illustrates the inner product and the angle among the semantic features \mathbf{x}_1 , \mathbf{x}_2 and \mathbf{x}_3 with the same input images. Table VI shows that even with the same input images, the inner products among the semantic features of different users are -1.0×10^{-3} , 7.0×10^{-3} and -2.8×10^{-4} , which approach zero. Moreover, the corresponding angles are 90.06° , 89.60° and 90.02° , which approach 90° . The results in Table VI verify the semantic features of multi-user are approximately orthogonal for the proposed SFDMA scheme.

Table VII further illustrates orthogonality through the image reconstruction performance using the same input images, which is shown in Fig. 9. As shown in Table VII, with the same inputs, the PSNRs of image reconstruction of User 1 and 2 decoding their intended signals are 25.72 dB and 25.68 dB, respectively, and the corresponding MS-SSIMs are 0.928 and 0.928, respectively, the decoded images are shown in Fig. 9(b) and 9(c), respectively.

Moreover, the PSNR and MS-SSIM of image reconstruction of User 1 decoding User 2's signal are 7.34dB and 0.066, respectively, and the decoded images are shown in Fig. 9(d).



Fig. 11: The decoded images of User 1 and 2 of the proposed SFDMA BC network.

The PSNR and MS-SSIM of image reconstruction of User 2 decoding User 1's signal are 7.20dB and 0.057, respectively, and the decoded images are shown in Fig. 9(e). The results in Table VII demonstrate that each user can accurately decode their intended signals, and cannot effectively decode the semantic information of other users, which also verify the semantic features of multi-user are approximately orthogonal for the proposed SFDMA scheme. Moreover, Table V also demonstrates the proposed SFDMA can protect the semantic information from being decoded by other users.

Fig. 10(a) illustrates PSNRs of Deep JSCC, Upper Bound and the proposed SFDMA for the semantic BC network versus SNR over Rayleigh channel with the training SNR = 0dB. Fig. 10(a) show that, as SNR increases, PSNRs of three schemes increase rapidly at first, and then slowly increases until it reaches the maximum value. Moreover, PSNRs of the proposed SFDMA scheme are higher than that of Deep JSCC, and approach to that of the Upper bound. Fig. 10(b) illustrates MS-SSIM of Deep JSCC, Upper Bound and the proposed SFDMA for the semantic BC network versus SNR over Rayleigh channel with the training SNR=5dB. Similar to Fig. 10(b), as SNR increases, MS-SSIMs of three schemes increase rapidly at first, and then slowly increases until it reaches the maximum value, and the PSNRs of the proposed SFDMA scheme are higher than that of Deep JSCC, and

approach to that of the Upper bound. Fig. 10(a) and Fig. 10(b) verify the proposed SFDMA scheme can effectively eliminate multi-user interference and improve image reconstruction tasks performance.

Furthermore, Fig. 11 illustrates the decoded images of User 1 and 2 of the proposed SFDMA BC network. Fig. 11(a) and 11(d) show the input images for User 1 and 2, respectively. Fig. 11(b) and 11(c) show the decoded image of SFDMA for User 1 with training and testing SNR=-5dB and SNR=5dB, respectively. Fig. 11(e) and 11(f) show the decoded image of SFDMA for User 2 with training and testing SNR=-5dB and SNR=5dB, respectively. Fig. 11 demonstrates that the proposed SFDMA can effectively support images transmission for multi-user BC networks.

D. Performance of power allocation schemes

Fig. 12 illustrates the cumulative distribution functions (CDFs) of classification accuracy of the fixed power allocation method and the proposed power allocation method, where the classification accuracy thresholds η_1 and η_2 are both 90%. Fig. 12 shows the classification accuracy of both two users under the optimal power allocation method is higher than the 90% threshold, which satisfies the inference tasks requirement, whereas the fixed power allocation method exhibits a probability of the classification accuracy falling below the threshold.

Fig. 13 illustrates the CDFs of MS-SSIM for the image reconstruction task. With MS-SSIM thresholds set at 0.77, the proposed method consistently maintains MS-SSIM consistently above the threshold. Additionally, its peak performance is comparable to that of the fixed power method, which often falls below the threshold. This demonstrates the superior performance of the proposed approach. Fig. 12 and Fig. 13 verifies that the propose power allocation method can effectively guarantee the QoS of semantic BC network.

VI. CONCLUSIONS

In this paper, we proposed a SFDMA scheme for the multi-user BC network with inference and image reconstruction tasks, in which the information of multiple users are encoded in distinguishable feature subspaces. The semantic encoded features of multiple users are simultaneously transmitted over the shared communication channel. Specifically, for our proposed SFDMA scheme, the encoded semantic features of multiple users are approximately orthogonal to each other, hence can be simultaneously transmitted in the same time-frequency resource. For inference tasks, we developed a RIB based SFDMA BC network to achieve a tradeoff between inference performance, data compression and multi-user interference. For image reconstruction tasks, we designed a Swin Transformer based SFDMA BC network, in which multi-user interference is significantly reduced, and each user can efficiently decode the intended images. Moreover, our proposed SFDMA scheme can protect the privacy of users' semantic information from being decoded by other users. Furthermore, we proposed the ABG formula to fit the relationship between task performance and SINR. Based on the ABG function, we proposed an optimal power allocation method for semantic BC networks with inference and reconstruction tasks. Our proposed power allocation method can effectively guarantee the performance requirements of semantic users in random fading channels.

REFERENCES

- [1] H. Liu, T. Qin, Z. Gao, T. Mao, K. Ying, Z. Wan, L. Qiao, R. Na, Z. Li, C. Hu *et al.*, "Near-space communications: The last piece of 6g space-air-ground-sea integrated network puzzle," *Space: Science & Technology*, vol. 4, p. 0176, 2024.
- [2] M. Wu, Z. Gao, Z. Wang, D. Niyato, G. K. Karagiannidis, and S. Chen, "Deep joint semantic coding and beamforming for near-space airship-borne massive mimo network," *arXiv preprint arXiv:2405.19889*, 2024.
- [3] I. F. Akyildiz, "Metaverse: Challenges for extended reality and holographic-type communication in the next decade," in *2022 ITU Kaleidoscope-Extended reality-How to boost quality of experience and interoperability*. IEEE, 2022, pp. 1–2.
- [4] E. Calvanese Strinati, S. Barbarossa, J. L. Gonzalez-Jimenez, D. Ktenas, N. Cassiau, L. Maret, and C. Dehos, "6G: The next frontier: From holographic messaging to artificial intelligence using subterahertz and visible light communication," *IEEE Veh. Technol. Mag.*, vol. 14, no. 3, pp. 42–50, Sep. 2019.
- [5] M. Yang, C. Bian, and H.-S. Kim, "Ofdm-guided deep joint source channel coding for wireless multipath fading channels," *IEEE Trans. Cognit. Commun. Netw.*, vol. 8, no. 2, pp. 584–599, Jun 2022.
- [6] S. Ihara, "On the capacity of channels with additive non-gaussian noise," *Information and Control*, vol. 37, no. 1, pp. 34–39, 1978.
- [7] B. Clerckx, H. Joudeh, C. Hao, M. Dai, and B. Rassouli, "Rate splitting for mimo wireless networks: A promising phy-layer strategy for lte evolution," *IEEE Commun. Mag.*, vol. 54, no. 5, pp. 98–105, May 2016.
- [8] Y. Mao and B. Clerckx, *Multiple Access Techniques*. Cham: Springer International Publishing, 2021, pp. 63–100. [Online]. Available: https://doi.org/10.1007/978-3-030-58197-8_3
- [9] B. Clerckx, Y. Mao, R. Schober, E. A. Jorswieck, D. J. Love, J. Yuan, L. Hanzo, G. Y. Li, E. G. Larsson, and G. Caire, "Is noma efficient in multi-antenna networks? a critical look at next generation multiple access techniques," *IEEE Open J. Commun. Soc.*, vol. 2, pp. 1310–1343, 2021.
- [10] W. Saad, M. Bennis, and M. Chen, "A vision of 6G wireless systems: Applications, trends, technologies, and open research problems," *IEEE Netw.*, vol. 34, no. 3, pp. 134–142, Oct. 2020.
- [11] P. Zhang, W. Xu, H. Gao, K. Niu, X. Xu, X. Qin, C. Yuan, Z. Qin, H. Zhao, J. Wei, and F. Zhang, "Toward wisdom-evolutionary and primitive-concise 6g: A new paradigm of semantic communication networks," *Engineering*, vol. 8, pp. 60–73, Jan. 2022.
- [12] H. Xie, Z. Qin, L. Geoffrey, Ye, and B.-H. Juang, "Deep learning enabled semantic communication systems," *IEEE Trans. Signal Process.*, vol. 69, pp. 2663–2675, Apr. 2021.
- [13] Z. Weng and Z. Qin, "Semantic communication systems for speech transmission," *IEEE J. Sel. Areas Commun.*, vol. 39, no. 8, pp. 2434–2444, Jun. 2021.
- [14] S. Ma, W. Qiao, Y. Wu, H. Li, G. Shi, D. Gao, Y. Shi, S. Li, and N. Al-Dhahir, "Task-oriented explainable semantic communications," *IEEE Trans. Wireless Commun.*, vol. 22, no. 12, pp. 9248–9262, Dec. 2023.
- [15] C.-H. Lee, J.-W. Lin, P.-H. Chen, and Y.-C. Chang, "Deep learning-constructed joint transmission-recognition for internet of things," *IEEE Access*, vol. 7, pp. 76547–76561, 2019.
- [16] D. Huang, F. Gao, X. Tao, Q. Du, and J. Lu, "Toward semantic communications: Deep learning-based image semantic coding," *IEEE J. Sel. Areas Commun.*, vol. 41, no. 1, pp. 55–71, 2022.
- [17] Q. Hu, G. Zhang, Z. Qin, Y. Cai, G. Yu, and G. Y. Li, "Robust semantic communications with masked vq-vae enabled codebook," *IEEE Trans. Wireless Commun.*, vol. 22, no. 12, pp. 8707–8722, Dec. 2023.
- [18] Y. M. J. Shao and J. Zhang, "Learning task-oriented communication for edge inference: An information bottleneck approach," *IEEE J. Sel. Areas Commun.*, vol. 40, no. 1, pp. 197–211, Jan. 2022.
- [19] S. Xie, S. Ma, M. Ding, Y. Shi, M. Tang, and Y. Wu, "Robust information bottleneck for task-oriented communication with digital modulation," *IEEE J. Sel. Areas Commun.*, vol. 41, no. 8, pp. 2577–2591, Aug. 2023.
- [20] N. Tishby, F. C. Pereira, and W. Bialek, "The information bottleneck method," 2000.
- [21] N. Farsad, M. Rao, and A. Goldsmith, "Deep learning for joint source-channel coding of text," in *Proc. IEEE Int. Conf. Acoust., Speech Signal Process. (ICASSP)*, 2018, pp. 2326–2330.
- [22] H. Xie and Z. Qin, "A lite distributed semantic communication system for internet of things," *IEEE J. Sel. Areas Commun.*, vol. 39, no. 1, pp. 142–153, Jan 2020.
- [23] K. Lu, R. Li, X. Chen, Z. Zhao, and H. Zhang, "Reinforcement learning-powered semantic communication via semantic similarity," *arXiv preprint arXiv:2108.12121*, 2021.
- [24] J. Xu, B. Ai, W. Chen, A. Yang, P. Sun, and M. Rodrigues, "Wireless image transmission using deep source channel coding with attention modules," *IEEE Trans. Circuits Syst. Video Technol.*, vol. 32, no. 4, pp. 2315–2328, 2022.
- [25] D. B. Kurka and D. Gündüz, "Bandwidth-agile image transmission with deep joint source-channel coding," *IEEE Trans. Wirel. Commun.*, vol. 20, no. 12, pp. 8081–8095, Jun. 2021.
- [26] E. Boursoulatzé, D. B. Kurka, and D. Gündüz, "Deep joint source-channel coding for wireless image transmission," *IEEE Trans. Cognit. Commun. Netw.*, vol. 5, no. 3, pp. 567–579, May. 2019.
- [27] T.-Y. Tung and D. Gündüz, "Deepwive: Deep-learning-aided wireless video transmission," *IEEE J. Sel. Areas Commun.*, vol. 40, no. 9, pp. 2570–2583, Sep. 2022.
- [28] C. V. N. Index, "Global mobile data traffic forecast update, 2016–2021 white paper," *Cisco: San Jose, CA, USA*, vol. 7, p. 180, 2017.
- [29] P. Jiang, C.-K. Wen, S. Jin, and G. Y. Li, "Wireless semantic communications for video conferencing," *IEEE Journal on Selected Areas in Communications*, vol. 41, no. 1, pp. 230–244, 2022.
- [30] H. Hu, X. Zhu, F. Zhou, W. Wu, R. Q. Hu, and H. Zhu, "One-to-many semantic communication systems: Design, implementation, performance evaluation," *IEEE Commun. Lett.*, vol. 26, no. 12, pp. 2959–2963, Dec. 2022.
- [31] H. Xie, Z. Qin, and G. Y. Li, "Task-oriented multi-user semantic communications for VQA," *IEEE Wireless Commun. Lett.*, vol. 11, no. 3, pp. 553–557, Mar. 2022.

- [32] Y. Zhang, W. Xu, H. Gao, and F. Wang, "Multi-user semantic communications for cooperative object identification," in *IEEE Int. Conf. Commun. Workshops (ICC Workshops)*, 2022, pp. 157–162.
- [33] P. Zhang, X. Xu, C. Dong, K. Niu, H. Liang, Z. Liang, X. Qin, M. Sun, H. Chen, N. Ma *et al.*, "Model division multiple access for semantic communications," *Frontiers of Information Technology & Electronic Engineering*, vol. 24, no. 6, pp. 801–812, 2023.
- [34] X. Luo, R. Gao, H.-H. Chen, S. Chen, Q. Guo, and P. N. Suganthan, "Multi-modal and multi-user semantic communications for channel-level information fusion," *IEEE Wireless Commun.*, pp. 1–18, 2022.
- [35] W. Zhang, K. Bai, S. Zeadally, H. Zhang, H. Shao, H. Ma, and V. C. M. Leung, "DeepMA: End-to-end deep multiple access for wireless image transmission in semantic communication," *IEEE Trans. Cogn. Commun. Netw.*, pp. 1 – 1, 2023.
- [36] Z. Liu, Y. Lin, Y. Cao, H. Hu, Y. Wei, Z. Zhang, S. Lin, and B. Guo, "Swin transformer: Hierarchical vision transformer using shifted windows," in *Proc. IEEE/CVF Conf. Comput. Vis. Pattern Recognit. (CVPR)*, 2021, pp. 10 012–10 022.
- [37] M. Courbariaux, I. Hubara, D. Soudry, R. El-Yaniv, and Y. Bengio, "Binarized neural networks: Training deep neural networks with weights and activations constrained to+ 1 or-1," *arXiv preprint arXiv:1602.02830*, 2016.
- [38] A. A. Alemi, I. Fischer, J. V. Dillon, and K. Murphy, "Deep variational information bottleneck," *arXiv preprint arXiv:1612.00410*, 2016.
- [39] Y. Li, B. Vucetic, Z. Zhou, and M. Dohler, "Distributed adaptive power allocation for wireless relay networks," *IEEE Trans. Wireless Commun.*, vol. 6, no. 3, pp. 948–958, 2007.
- [40] H. Xie, Z. Qin, G. Y. Li, and B.-H. Juang, "Deep learning enabled semantic communication systems," *IEEE Transactions on Signal Processing*, vol. 69, pp. 2663–2675, 2021.
- [41] L. Deng, "The mnist database of handwritten digit images for machine learning research [best of the web]," *IEEE signal processing magazine*, vol. 29, no. 6, pp. 141–142, 2012.
- [42] Z. Liu, P. Luo, X. Wang, and X. Tang, "Deep learning face attributes in the wild," in *Proceedings of International Conference on Computer Vision (ICCV)*, December 2015.
- [43] L. Van der Maaten and G. Hinton, "Visualizing data using t-SNE." *J. Mach. Learn. Res.*, vol. 9, no. 11, 2008.